RSC Advances

ROYAL SOCIETY OF CHEMISTRY

www.rsc.org/advances

RSC Advances

RSCPublishing

ARTICLE

Ni-Cu alloy nanoparticles loaded on various metal oxides acting as efficient catalysts for photocatalytic H_2 evolution

Cite this: DOI: 10.1039/x0xx00000x

Received 00th March 2015,
Accepted 00th xxxx 2015

DOI: 10.1039/x0xx00000x

www.rsc.org/

Yusuke Yamada,*[ab] Shinya Shikano[a] and Shunichi Fukuzumi*[acd]

Catalysis of Al_2O_3-SiO_2, TiO_2, SiO_2 and CeO_2 (MOx) impregnated with pre-formed Ni-Cu alloy nanoparticles (Ni-CuNPs/MOx) for photocatalytic hydrogen (H_2) evolution was compared with that of MOx impregnated with Ni^{2+} and Cu^{2+} ions followed by reduction (Ni-Cu/MOx). The photocatalytic H_2 evolution was conducted by photoirradiation (λ > 340 nm) of a deaerated mixed solution of [illegible] phthalate buffer (pH 4.5) and acetonitrile [1:1 (v/v)] containing β-dihydronicotinamide adenine dinucleotide (NADH), 2-phenyl-4-(1-naphthyl)quinolinium ion ($QuPh^+$–NA), and Ni-CuNPs/MOx or [illegible] Cu/MOx as an electron donor, a photosensitiser and an H_2-evolution catalyst, respectively. Ni-CuNPs/Al_2O_3-SiO_2 exhibited activity for the photocatalytic H_2 evolution, whereas Ni-Cu/Al_2O_3-SiO_2 showed no activity. Such precursor dependent catalysis can be elucidated by the ion-exchangeable nature and high surface area of Al_2O_3-SiO_2, on which Ni-Cu alloy particles hardly form from metal salts. On the other hand, Ni-Cu/TiO_2 and Ni-Cu/SiO_2 exhibited higher activity than Ni-CuNPs/TiO_2 and Ni-CuNPs/SiO_2, respectively, resulting from formation of smaller Ni-Cu alloy nanoparticles on TiO_2 and SiO_2 by reducing Ni^{2+} and Cu^{2+} on the surfaces. When CeO_2 was used as the support, no catalytic activity was observed for either Ni-CuNPs/CeO_2 or Ni-Cu/CeO_2. Kinetic study for thermal H_2 evolution suggested that Ni-CuNPs were severely deactivated for H_2 evolution by being loaded on CeO_2.

1. Introduction

Hydrogen (H_2) has been regarded as the most promising energy carrier of the next generation,[1-3] however, most part of H_2 supplied to chemical industry is currently produced by the steam forming of fossil fuels such as natural gas, which is a large energy consuming process and emitting carbon dioxide as a main by-product.[4] It is highly desired that H_2 is produced from renewable chemicals by utilizing natural energy.[5] In this context, H_2 production utilizing solar energy has attracted much attention in this research field.[6-13] Visible light-driven photocatalytic H_2-evolution systems composed of a photosensitiser, an electron relay and an H_2-evolution catalyst have so far been extensively studied.[14–25] Recently, efficient photocatalytic H_2-evolution systems were developed by employing electron donor–acceptor linked dyads,[26–32] which form long-lived electron transfer states under photoirradiation.[33–35] The long lifetime of the electron-transfer states allows to eliminate electron relays in the H_2-evolution systems.[27–32]

Pt nanoparticles has been widely used as a high performance H_2-evolution catalyst,[36,37] however, Pt is a most expensive metal because of its limited reserve.[38] Thus, reduction of usage of precious metals and development of alternative catalysts composed of cheaper metals are highly demanded. For reduction of using amount of precious metals, Ru nanoparticles supported on a silica support have been developed.[39] As a catalyst using a base metal, Ni nanoparticles has been reported although catalytic activity was half that of Pt nanoparticles.[40] Recently, Ni and Cu loaded on silica or titania prepared by a conventional impregnation method using $Ni(NO_3)_2$ and $Cu(NO_3)_2$ as precursors followed by reduction have been reported to exhibit high catalytic activity with a synergistic effect.[41] Although the catalytic activity highly depends on the preparation procedures and supports of the catalysts,[41] requisites to obtain the synergistic effect between Ni and Cu and the origin of the support effect have yet to be clarified.

We report herein catalytic activity of Ni-Cu alloy nanoparticles, which were prepared *ex situ* by thermal decomposition of $Ni(acac)_2$ and $Cu(acac)_2$ (acac = acetylacetonato), loaded on a metal oxide support chosen from SiO_2, TiO_2, Al_2O_3-SiO_2 and CeO_2 (MOx) for photocatalytic H_2 evolution. The photocatalytic H_2 evolution was conducted by photoirradiation (λ > 340 nm) of a mixed solution of [illegible] phthalate buffer (pH 4.5) and MeCN containing β-

dihydronicotinamide adenine dinucleotide (NADH), 2-phenyl-4-(1-naphthyl)quinolinium ion ($QuPh^+$–NA) and Ni-CuNPs/MOx as an electron donor, a photosensitiser and an H_2-evolution catalyst, respectively. The chemical structure of $QuPh^+$–NA and the overall photocatalytic cycle of H_2 evolution are depicted in Scheme 1. The catalytic activity of Ni-CuNPs/MOx was compared with that of Ni-Cu/MOx, which are prepared by the impregnation method using $Ni(NO_3)_2$ and $Cu(NO_3)_2$ as precursors to clarify the requisites for high catalytic activity with each support.

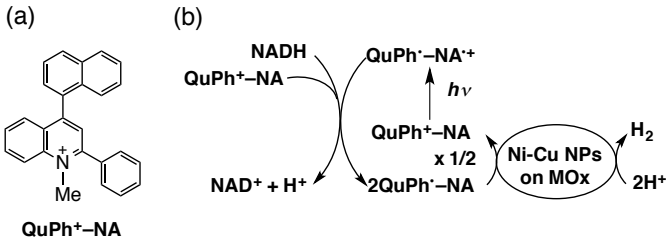

Scheme 1 (a) Molecular structure of $QuPh^+$–NA and (b) the overall photocatalytic cycle of H_2 evolution

2. Results and discussion

2.1 Effect of Ni-Cu alloy formation on catalysis

Ni and Ni-Cu alloy nanoparticles (NiNPs and Ni-CuNPs) were prepared by thermal decomposition of $Ni(acac)_2$ and/or $Cu(acac)_2$ in deaerated oleylamine and 1-ocatadecene at 230 °C by changing the ratio of Ni/Cu between 1/0 and 5/5.[42] Cu nanoparticles (CuNPs) were obtained by $Cu(OAc)_2$ reduction by $NaBH_4$ in the presence of polyvinylpyrrolidone (PVP).[43] The molar ratio of Ni/Cu in the Ni-CuNPs determined by the X-ray fluorescence measurements was 55/45. The particles sizes of the as-prepared nanoparticles determined by dynamic laser scattering (DLS) were 25, 15 and 50 nm for NiNPs, Ni-CuNPs and CuNPs, respectively (Fig. S1). The sizes of NiNPs and Ni-CuNPs agreed with those determined by the TEM observation (Figs. 1b and 1c), however, the sizes of CuNPs determined by TEM were larger than 100 nm (Fig. 1a), which is double of those determined by DLS measurements. Growing of CuNPs resulted from the exposure to the electron beam for TEM observation, or intrinsic instability of CuNPs after removal of excess stabiliser during washing process.

Alloy formation in Ni-CuNPs was clearly confirmed by powder X-ray diffraction measurements. In general, both Cu and Ni metals take the face–centred–cubic structure.[44] The reflection peaks from (111) surfaces of CuNPs and NiNPs appeared at $2\theta = 43.4°$ and 44.7°, respectively (Figs. 1d and 1f), which are agreed with the values reported for Cu metal and Ni metal, 43.38° and 44.53°, respectively,[44] although the peak position of CuNPs is inaccurate owing to concomitant formation of Cu_2O species as evidenced by the peak appeared at 36.58°.[44] The (111) diffraction peak of Ni-CuNPs appeared at 43.5°, which is in between those from NiNPs and CuNPs, without an accompanied peak. Thus, Ni-CuNPs used as a precursor for preparation of Ni-CuNPs/MOx (*vide infra*) are

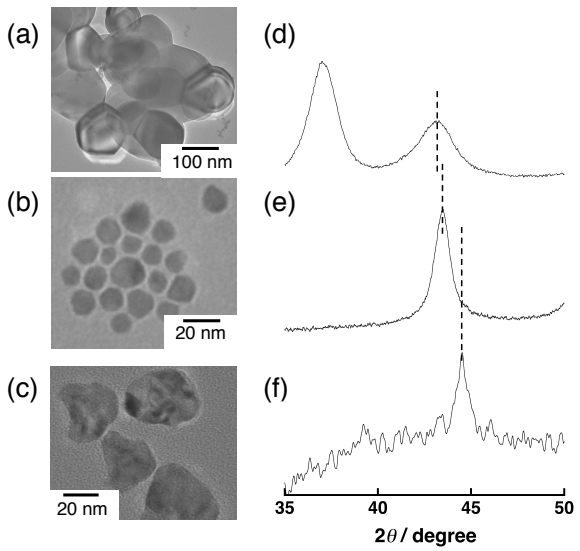

Fig. 1 TEM images and powder X-ray diffraction peaks of (a,d) Cu nanoparticles, (b,e) Ni-Cu alloy nanoparticles and (c,f) Ni nanoparticles from (111) plane.

regarded as Ni-Cu alloy with the size of 15 nm.

The instability of CuNPs prevents their direct use for photocatalytic H_2 evolution. Thus, NiNPs, CuNPs and Ni-CuNPs were loaded on TiO_2 by the impregnation method to compare catalysis of Ni-CuNPs/TiO_2 for photocatalytic H_2 evolution with those of NiNPs/TiO_2 and CuNPs/TiO_2. The photocatalytic H_2 evolution was conducted by photoirradiation ($\lambda > 340$ nm) of a deaerated mixed solution (2.0 mL) of a phthalate buffer (50 mM, pH 4.5) and acetonitrile (MeCN) [1:1 (v/v)] containing NADH (1.0×10^{-3} M), $QuPh^+$–NA (8.8×10^{-4} M) and Ni-CuNPs/TiO_2, NiNPs/TiO_2 or CuNPs/TiO_2 (100 mg L^{-1}). Continuous H_2 evolution was observed for the reaction system employing Ni-CuNPs/TiO_2 with an H_2-evolution rate of 0.9 μmol h^{-1}, whereas no or insignificant amount of H_2 evolution was observed for the reaction systems employing CuNPs/TiO_2 and NiNPs/TiO_2 (Fig. 2). Thus, alloy formation of

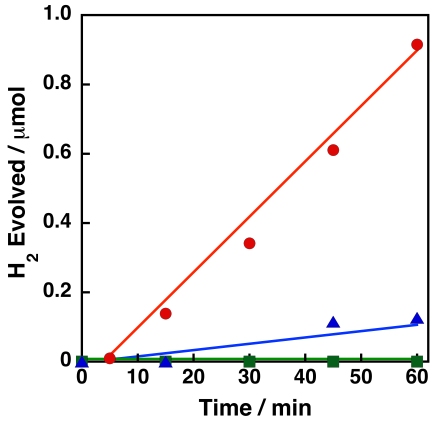

Fig. 2 Time courses of H_2 evolution under photoirradiation ($\lambda > 340$ nm) of an N_2-saturated mixed solution (2.0 mL) of a phthalate buffer (pH 4.5) and MeCN [1:1 (v/v)] containing $QuPh^+$–NA (8.8×10^{-4} M), NADH (1.0×10^{-3} M) and 3.5 wt% Ni-CuNPs/TiO_2 (red circle), 1.3 wt% NiNPs/TiO_2 (green square) or (c) 3.2 wt% CuNPs/TiO_2 (blue triangle) (100 mg L^{-1}).

Ni and Cu is necessary for high catalytic activity. The high catalytic activity could result from the optimisation of metal-hydrogen bond strength, because the nickel-hydrogen bond seems too strong, on the contrary, the copper-hydrogen bond seems too weak for H_2 evolution as predicted by the density functional theory (DFT) calculations.[45] The induction period (5 min) before H_2 evolution may result from the reduction of native oxide formed on the surface of Ni-CuNPs.

2.2 Precursors effect of Ni–Cu alloy nanoparticles loaded on TiO_2 and SiO_2 on photocatalytic H_2 evolution

The surface structures of Ni-CuNPs/TiO_2 and Ni-Cu/TiO_2 were observed by a transmission electron microscope (TEM). Ni-CuNPs/TiO_2 were prepared by the impregnation method using pre-formed Ni-CuNPs as a precursor, on the other hand, Ni-Cu/TiO_2 samples were prepared by the impregnation method using $Ni(NO_3)_2$ and $Cu(NO_3)_2$ as precursors with the reductive treatment. Particles with the size of 10-20 nm were observed on TiO_2 surfaces of Ni-CuNPs/TiO_2 (Fig. 3a), whilst smaller particles with the size of ~5 nm were observed on TiO_2 surfaces of Ni-Cu/TiO_2 (Fig. 3c). Formation of Ni-Cu alloy for both samples was evidenced by identical peak positions of the diffraction peaks around 43.5° in powder XRD patterns (Figs. 3b and 3d). The loading amounts of Ni-Cu alloy were determined by X-ray fluorescence measurements as 3.5 and 3.0 wt% for Ni-CuNPs/TiO_2 and Ni-Cu/TiO_2, respectively.

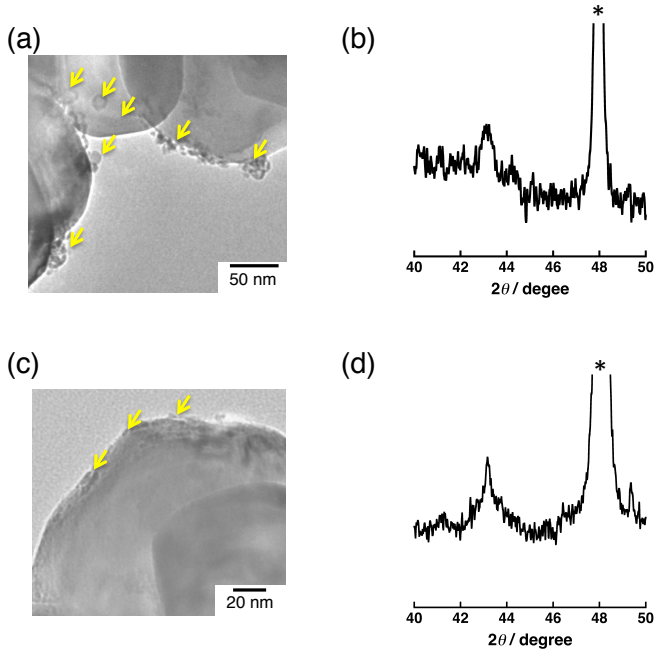

Fig. 3 (a,c) TEM images and (b,d) powder X-ray diffraction peaks of Ni-Cu/TiO_2 prepared by the impregnation method using (a, b) Ni-Cu nanoparticles or (c,d) $Ni(NO_3)_2$ and $Cu(NO_3)_2$. The diffraction peaks with the "*" mark originate from the TiO_2 support.

Photocatalytic H_2 evolution was performed by employing Ni-Cu/TiO_2 as an H_2-evolution catalyst (Fig. 4a, square). The average H_2-evolution rate for the reaction time between 5 to 30 min was 1.5 μmol h^{-1} with an H_2 yield higher than 80%. The photocatalytic H_2 evolution was also examined by employing Ni-CuNPs/TiO_2 instead of Ni-Cu/TiO_2 under otherwise the same conditions (Fig. 4a, circle). The H_2-evolution rate and H_2 yield were 0.82 μmol h^{-1} and 50%, respectively, suggesting that Ni-Cu/TiO_2 is superior to Ni-CuNPs/TiO_2 in terms of the H_2-evolution rate and H_2 yield. The lower catalytic activity of Ni-CuNPs/TiO_2 resulted from larger particles size as implied previously where the optimum loading amount of Ni and Cu is between 3-4 wt% and further increase in the loading amount resulted in lower catalytic activity.[41]

More obvious precursor effect was observed when SiO_2 was employed as the support. Ni-Cu/SiO_2 prepared by using $Ni(NO_3)_2$ and $Cu(NO_3)_2$ exhibited high catalytic activity in terms of an H_2 yield higher than 70% and an H_2-evolution rate of 1.3 μmol h^{-1} (Fig. 4b, square). On the other hand, Ni-CuNPs/SiO_2 exhibited a lower H_2 yield of 20% and an H_2-evolution rate of 0.2 μmol h^{-1} (Fig. 4b, circle). TEM observations suggest that the sizes of Ni-CuNPs supported on SiO_2 were ~2 nm and 10-15 nm for Ni-Cu/SiO_2 and Ni-CuNPs/SiO_2, respectively (Fig. S2). Thus, decreasing the size of Ni-CuNPs would be important for catalysis improvement. Additionally, the higher catalytic activity of Ni-CuNPs/TiO_2 than that of Ni-CuNPs/SiO_2 may result from the higher reducibility of TiO_2.[41]

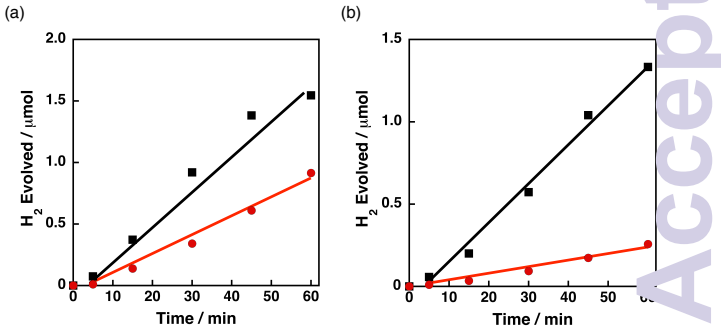

Fig. 4 Time courses of H_2 evolution under photoirradiation (λ > 340 nm) of a deaerated mixed solution (2.0 mL) of a phthalate buffer (pH 4.5) and MeCN [1:1 (v/v)] containing $QuPh^+$–NA (8.8×10^{-4} M), NADH (1.0×10^{-3} M) and (a) 3 wt% Ni-Cu/TiO_2 (100 mg L^{-1}, black square) and 3.5 wt% Ni-CuNPs/TiO_2 (100 mg L^{-1}, red circle) and (b) 3 wt% Ni-Cu/SiO_2 (100 mg L^{-1}, black square) and 3.5 wt% Ni-CuNPs/SiO_2 (100 mg L^{-1}, red circle).

2.3 Photocatalytic H_2 evolution with Ni-CuNPs supported on Al_2O_3-SiO_2

On the contrary to Ni-CuNPs/TiO_2 and Ni-CuNPs/SiO_2, Ni-CuNPs/Al_2O_3-SiO_2 exhibited higher catalytic activity for the photocatalytic H_2 evolution than Ni-Cu/Al_2O_3-SiO_2. H_2-evolution rate was 0.6 μmol h^{-1} for the photocatalytic H_2-evolution system employing Ni-CuNPs/Al_2O_3-SiO_2, which was prepared by using pre-formed Ni-Cu nanoparticles, as an H_2 evolution catalyst under otherwise the same reaction condition for Ni-CuNPs/TiO_2. The H_2-evolution rate was slightly slower but comparable to that of Ni-CuNPs/TiO_2 (0.9 μmol h^{-1}). On the contrary, Ni-Cu/Al_2O_3-SiO_2, which was prepared by the impregnation method using $Ni(NO_3)_2$ and $Cu(NO_3)_2$ as precursors with the reductive treatment, showed insignificant

activity for the photocatalytic H_2 evolution (Fig. 5). Thus, the structure of Ni and Cu species on the surface of Al_2O_3-SiO_2 should be different for these catalysts.

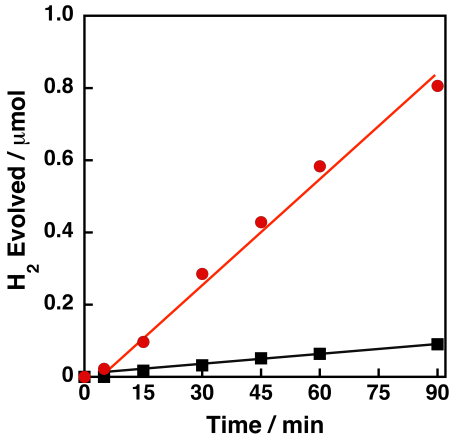

Fig. 5 Time courses of H_2 evolution under photoirradiation (λ > 340 nm) of a deaerated mixed solution of a phthalate buffer and MeCN [1:1 (v/v)] containing $QuPh^+$–NA (8.8 x 10^{-4} M), NADH (1.0 x 10^{-3} M) and 3 wt% Ni-Cu/Al_2O_3-SiO_2 (100 mg L^{-1}, black square) or 6.5 wt% Ni-Cu/Al_2O_3-SiO_2 (100 mg L^{-1},red circle).

The structure of Ni-CuNPs loaded on Al_2O_3-SiO_2 was confirmed by TEM observations. As shown in Fig. 6a, deposition of Ni-CuNPs with the size of 10-20 nm on Al_2O_3-SiO_2 surfaces was observed as the cases of Ni-CuNPs/TiO_2 and Ni-CuNPs/SiO_2. Fewer and much smaller Ni and/or Cu metal

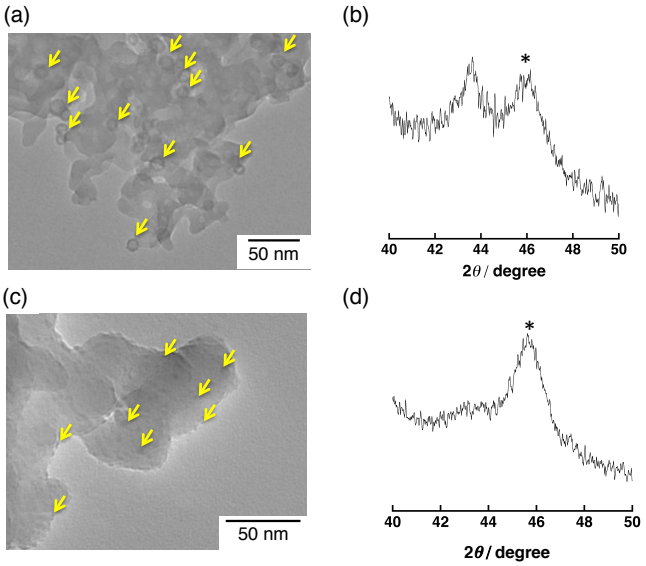

Fig. 6 (a,c) TEM images and (b,d) powder X-ray diffraction peaks of Ni-Cu/Al_2O_3-SiO_2 prepared by the impregnation method using (a, b) Ni-Cu nanoparticles or (c,d) $Cu(NO_3)_2$ and $Ni(NO_3)_2$. The diffraction peaks with the "*" mark originate from the Al_2O_3-SiO_2 support.

nanoparticles on Al_2O_3-SiO_2 were observed for Ni-Cu/Al_2O_3-SiO_2 as the cases of Ni-Cu/TiO_2 and Ni-Cu/SiO_2. The XRD peak around 2θ = 43° assignable to metal particles was observed for Ni-CuNPs/Al_2O_3-SiO_2, however, a weak shoulder peak was observed for Ni-Cu/Al_2O_3-SiO_2, suggesting that little formation of metal particles including Ni, Cu and Ni-Cu alloy on Ni-Cu/Al_2O_3-SiO_2. Thus, the low catalytic activity of Ni-Cu/Al_2O_3-SiO_2 may be ascribed to little formation of Ni-Cu alloy particles on Al_2O_3-SiO_2.

Little formation of Ni-CuNPs on Ni-Cu/Al_2O_3-SiO_2 can be explained by the presence of cation exchange sites of Al_2O_3-SiO_2 with a high surface area. In an aqueous solution, Ni^{2+} and Cu^{2+} ions can be adsorbed on cation exchange sites by electrostatic interaction. The strongly adsorbed metal ions are hardly reduced to form metal nanoparticles on the surfaces of Al_2O_3-SiO_2 with a high surface area (Scheme 2). When a support has no cation exchange sites, physisorbed Ni^{2+} and Cu^{2+}, which weakly bound to the surfaces, can move around to form Ni-Cu alloy particles during the heat and reduction treatment.

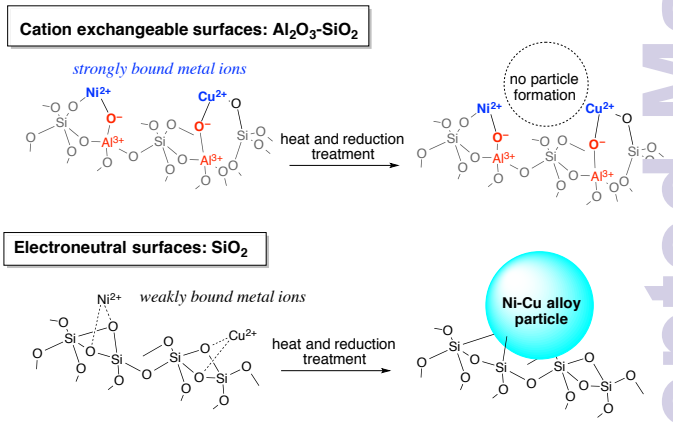

Scheme 2 Formation of Ni-CuNPs on electroneutral surfaces and non-formation of Ni-CuNPs on cation exchangeable surfaces

2.4 Photocatalytic H_2 evolution with Ni-CuNPs supported on CeO_2

Both Ni-Cu/CeO_2 and Ni-CuNPs/CeO_2 exhibited very low catalytic activity for the photocatalytic H_2 evolution (Fig. 7),

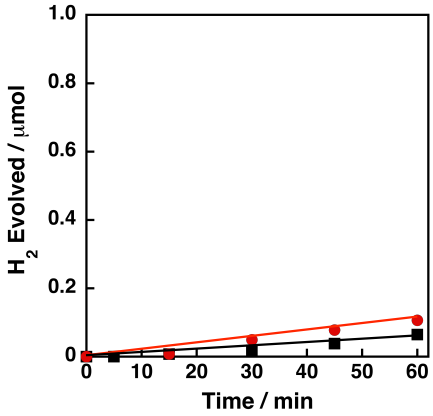

Fig. 7 Time courses of H_2 evolution under photoirradiation (λ > 340 nm) of a deaerated mixed solution of a phthalate buffer and MeCN [1:1 (v/v)] containing $QuPh^+$–NA (8.8 x 10^{-4} M), NADH (1.0 x 10^{-3} M) and Ni-Cu/CeO_2 (100 mg L^{-1}) prepared by impregnation method using Ni and Cu salts (black square, 3wt%) and Ni-Cu nanoparticles (red circle, 2.4wt%).

although TEM measurements for Ni-CuNPs/CeO_2 indicated that Ni-CuNPs were successfully loaded on CeO_2 surfaces as same as Ni-CuNPs/Al_2O_3-SiO_2 (Fig. S3). However, the H_2 yields calculated from the amount of NADH in the reaction solutions were less than 5% and the H_2-evolution rates were lower than 0.1 μmol h^{-1} for both Ni-Cu/CeO_2 and Ni-CuNPs/CeO_2. There are two possible reasons for such low catalytic activity of Ni-Cu/CeO_2. One is the overlapping of absorption of CeO_2 and $QuPh^+$–NA (Fig. 8). Stronger light absorption (< 460 nm) by CeO_2 disturbs the light absorption by $QuPh^+$–NA to form $QuPh^•$–NA. The other possible reason is electronic interaction between CeO_2 and Ni-CuNPs. High mobility of lattice oxygen of CeO_2 may result in oxidation of Ni-CuNPs, which is unsuitable for proton reduction.

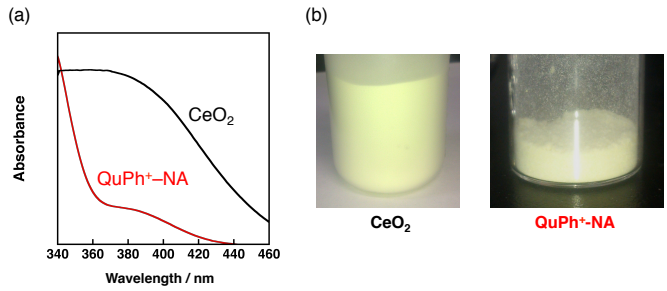

Fig. 8 (a) Diffuse reflectance UV-vis spectra of CeO_2 (black) and $QuPh^+$–NA (red) and (b) photographs of CeO_2 and $QuPh^+$–NA.

The rate-determining step of the photocatalytic H_2 evolution is the proton reduction on a catalyst surface or H_2 evolution. To evaluate the proton reduction and H_2-evolution catalysis of Ni-CuNPs/CeO_2 under thermal reaction conditions, the proton reduction by $QuPh^•$–NA was executed as follows: $QuPh^•$–NA was generated by photoirradiation of a mixed solution containing $QuPh^+$–NA in the presence of NADH. After $QuPh^•$–NA formed, an aliquot of dispersion containing an H_2-evolution catalyst such as Ni-CuNPs/CeO_2 was injected to the solution in the dark. When Ni-Cu/TiO_2 was employed as the H_2-evolution catalyst, a considerable amount of H_2 evolution was observed within 15 min (Fig. 9, circle). On the other hand, much slower H_2 evolution was observed when Ni-Cu/CeO_2 or Ni-CuNPs/CeO_2 was employed as the catalyst (Fig. 9, square and triangle). The slower H_2 evolution suggests that Ni-CuNPs are deactivated on the surfaces of CeO_2. Thus, electronic interaction between CeO_2 and Ni-CuNPs is the predominant reason for the low catalytic activity of Ni-CuNPs/CeO_2.

3. Conclusions

Various metal oxide catalysts supporting Ni and Cu alloy nanoparticles (Ni-CuNPs) were prepared and employed for the photocatalytic H_2 evolution. Catalytically active smaller Ni-CuNPs were formed on TiO_2 and SiO_2 by impregnation of $Ni(NO_3)_2$ and $Cu(NO_3)_2$ followed by the reduction. On the contrary, Ni-CuNPs formation was not observed when Al_2O_3-SiO_2 was employed as a support instead of TiO_2 or SiO_2. To

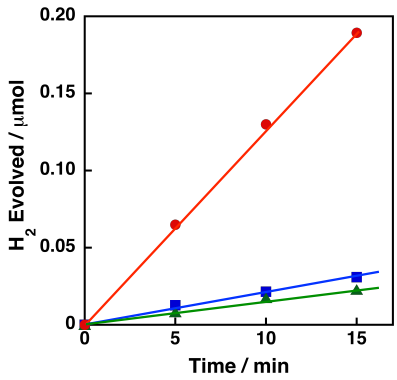

Fig. 9 Time courses of H_2 evolution by the thermal reduction of protons by $QuPh^•$–NA (0.44 mM) in the presence of 3 wt% Ni-Cu/TiO_2 (red circle) and Ni-Cu/CeO_2 prepared by the impregnation method using Ni-Cu nanoparticles (green triangle, 2.4 wt%) or $Ni(NO_3)_2$ and $Cu(NO_3)_2$ as precursors (blue square, 3 wt%).

achieve high catalytic activity, pre-formed Ni-CuNPs (Ni-Cu/Al_2O_3-SiO_2) should be used as a precursor of Ni-CuNPs/Al_2O_3-SiO_2. These results clearly indicate t importance of Ni-Cu alloy formation, in which metal-hydrogen bond strength may be optimized. When CeO_2 was used as t support, no active catalyst for H_2 evolution was obtained irrespective of precursors, suggesting that CeO_2 is unsuitable support for Ni-CuNPs acting as H_2 evolution catalysts. By employing pre-formed Ni-CuNPs as a precursor of a impregnation method, the synergistic effect between Ni and Cu and the support effect can be considered separately.

4. Experimental section

4.1 Materials

All chemicals were obtained from chemical companies and used without further purification. SiO_2 (10-20 nm), TiO_2 (anatase), nickel acetylacetonate [$Ni(acac)_2$] and oleylamin (70%) were purchased from Sigma-Aldrich. Copper nitrate, nickel nitrate, copper acetate [$Cu(OAc)_2$], sodium hydroxide and sodium aluminate were obtained from Wako Pure Chemical Industries. Copper acetylacetonate [$Cu(acac)_2$], 1-octadecene, polyvinylpyrrolidone (PVP) and β-dihydronicotinamide adenine dinucleotide disodium salt (reduced form) (NADH) were obtained from Tokyo Chemical Industry. Acetonitrile was obtained from Nacalai Tesque. CeO_2 was provided by Daiichi Kigenso Kagaku Kogyo Co., Ltd. 2-Phenyl-4-(1-naphthyl)quinolinium perchlorate ($QuPh^+$–NA),[34] Ni-Cu alloy nanoparticles,[42] Ni nanoparticles,[42] Cu nanoparticles,[43] and Al_2O_3-SiO_2[46,47] were prepared by literature methods. Purified water was provided by using a Millipore DIRECT-Q UV3 water purification system (18.2 MΩ cm).

4.2 Preparation of Ni-Cu alloy nanoparticles[42]

Ni-Cu alloy nanoparticles were prepared by a literature method.[42] $Ni(acac)_2$ (26 mg, 0.10 mmol) and $Cu(acac)_2$ (26 mg, 0.10 mmol) were dissolved in dry oleylamine (1.0 mL) at 85 °C under an Ar atmosphere. A mixed solution of oleylamine (1 mL) and 1-octadecene (10 mL) in a 50 mL three-neck roun bottom flask was degassed under reduced pressure for 30 min at

140 °C to remove water and oxygen, then heated to 230 °C (ramp rate: 10 °C min^{-1}) under an Ar atmosphere. The solution containing metal precursors was injected into the mixed solvents in 20 s, and was allowed to further react for 10 min at the temperature under an Ar atmosphere. After cooled to room temperature, the obtained suspension was centrifuged (9000 rpm, 10 min) to separate black precipitates. The black precipitates were washed three times by dispersion/precipitation (*n*-hexane/ethanol) cycles. The final product was dispersed in *n*-hexane (5 mL).

4.3 Preparation of Ni nanoparticles[42]

$Ni(acac)_2$ (51 mg, 0.20 mmol) was dissolved in dry oleylamine (1.0 mL) at 85 °C under an Ar atmosphere. A mixed solution of oleylamine (15 mL) and 1-octadecene (5 mL) in a 50 mL three-neck round-bottom flask was degassed under reduced pressure for 30 min at 140 °C to remove water and oxygen, then heated to 230 °C (ramp rate: 5 °C min^{-1}) under an Ar atmosphere. The solution of the nickel precursor was injected into the mixed solvents in 20 s, and allowed to react for 5 min at this temperature under an Ar atmosphere. After cooled to room temperature, the obtained suspension was centrifuged (9000 rpm, 10 min) to separate black precipitates. The black precipitates were washed three times by dispersion/precipitation (*n*-hexane/ethanol) cycles. The final product was dispersed in *n*-hexane (5 mL).

4.4 Preparation of Cu nanoparticles[43]

$Cu(OAc)_2$ (60 mg, 0.30 mmol) and PVP (0.40 g) were dissolved in water (20 mL) in a 50 mL three-neck round-bottom flask at room temperature. Then, an aqueous solution of $NaBH_4$ (11 mg, 0.30 mmol) and NaOH (12 mg, 0.30 mmol) was injected into the $Cu(OAc)_2$/PVP aqueous solution and stirred for 15 min under an Ar atmosphere at room temperature. After the reaction, acetone was added to cause flocculation and then the suspension was centrifuged (9000 rpm, 10 min) to separate black precipitates. The black precipitates were washed three times by dispersion/precipitation (acetone/ethanol) cycles. The final product was dispersed in ethanol (5 mL).

4.5 Preparation of Al_2O_3-SiO_2[46,47]

SiO_2 was suspended in an aqueous solution (50 mL) containing sodium aluminate (1.3 g, 16 mmol) and stirred for 20 h at room temperature. The precipitate was collected by filtration and dried at 120 °C. The dried sample was calcined at 550 °C (ramp rate: 5 °C min^{-1}) for 6 h in air.

4.6 Preparation of Ni-Cu loaded on metal oxides by using $Ni(NO_3)_2$ and $Cu(NO_3)_2$ as precursors

A typical procedure for the preparation of metal oxides loading Ni and Cu by an impregnation method is as follows: A metal oxide support (350 mg) was immersed in an aqueous solution containing $Ni(NO_3)_2{\cdot}6H_2O$ (27 mg, 92 mmol) and $Cu(NO_3)_2{\cdot}3H_2O$ (21 mg, 85 mmol) and sonicated for 30 min. The obtained catalyst precursor was dried at 60 °C in an oven and calcined at 350 °C (ramp rate: 5 °C min^{-1}) for 4 h under air. The obtained powder was immersed in an aqueous solution containing $NaBH_4$ to reduce oxides of Cu and Ni before catalysis evaluation.

4.7 Preparation of Ni-Cu alloy nanoparticles loaded on metal oxides

A metal oxide support (50 mg) was immersed in a hexane solution (30 mL) containing Ni-CuNPs (1.5 mL of the stock solution) and sonicated for 30 min. The obtained catalyst precursor was dried at 60 °C in an oven and calcined at 350 °C (ramp rate: 5 °C min^{-1}) for 4 h in air. The obtained powder was soaked in an ethanol solution containing $NaBH_4$ to reduce oxides of Cu and Ni before catalysis evaluation. The loading amount of Ni-Cu was determined by X-ray fluorescence measurements.

4.8 Transmission electron microscopy (TEM)

The sizes and shapes of nanoparticles were determined from bright field images using a JEOL JEM-2100 that has a thermal field emission gun with an accelerating voltage of 200 kV. The observed samples were prepared by dropping a dispersion of catalysts and allowing the solvent to evaporate and then scooped up with an amorphous carbon supporting film on a Cu grid.

4.9 Catalysts characterisation by powder X-ray diffraction, diffused reflectance UV-vis spectroscopy and dynamic laser scattering

X-ray diffraction patterns were recorded by a Rigaku MiniFlex 600. Incident X-ray radiation was produced by a Cu X-ray tube operating at 40 kV and 15 mA with Cu $K\alpha$ radiation of 1.54 Å. The scanning rate was 2° min^{-1} from 10° to 80° in 2θ. The diffuse reflectance UV-vis spectra were recorded with a Jasco V-670 spectrophotometer equipped with an integrating sphere module (SIN-768). Reflectance obtained for each sample was converted to $f(R_\infty)$ values according to the Kubelka-Munk theory, $f(R_\infty) = (1- R_\infty)^2 / 2R_\infty$, where R_∞ is the reflectance of the sample layer. $BaSO_4$ was used for back ground spectra measurements. Dynamic light scattering (DLS) measurements were performed with a Zetasizer Nano ZS instrument (Malvern Instruments Ltd., U.S.A.).

4.10 N_2 adsorption for BET surface area determination

Nitrogen adsorption-desorption at 77 K was performed with a Belsorp-mini (BEL Japan, Inc.) within a relative pressure range from 0.01 to 101.3 kPa. A sample mass of ~100 mg was used for adsorption analysis after pretreatment at 120 °C for 1 h under vacuum conditions and kept in N_2 atmosphere until N_2-adsorption measurements. The samples were exposed to a mixed gas of He and N_2 with a programmed ratio and adsorbed amount of N_2 was calculated from the change of pressure in a cell after reaching the equilibrium (at least 5 min). The surface area of each catalyst was determined by the Brunauer-Emmett-Teller (BET) method for multiple N_2 adsorption amounts under the conditions of partial pressure less than 0.3. The Brunauer-Emmett-Teller (BET) surface areas of TiO_2, SiO_2, SiO_2-Al_2O_3, CeO_2 were determined to be 6.8, 52, 118 and 162 m^2 g^{-1}, respectively.

4.11 Photocatalytic H_2 evolution

A mixed solution (2.0 mL) of a phthalate buffer (pH 4.5) and MeCN [1:1 (v/v)] containing $QuPh^+$–NA (0.88 mM), NADH (1.0 mM) and an H_2-evolution catalyst was flushed with N_2 gas. The solution was then irradiated for a certain time with a xenon

lamp (Ushio Optical, Model X SX-UID 500X AMQ) through a colour filter glass (Asahi Techno Glass L39) transmitting $\lambda >$ 340 nm at room temperature. After 1 min stirring in the dark, gas in a headspace was analysed by Shimadzu GC-14B gas chromatography (detector: TCD, column temperature: 50 ºC, column: active carbon with the particle size 60-80 mesh, carrier gas: N_2 gas) to determine the amount of evolved H_2.

4.12 H_2 evolution with $QuPh^{\bullet}$–NA in the dark[39,41]

Typically, a mixed solution (2.0 mL) of a deaerated phthalate buffer (pH 4.5) and MeCN [1:1 (v/v)] containing $QuPh^{+}$–NA (0.44 mM) and NADH (1.0 mM) was photoirradiated for 5 min with a Xe lamp through a colour filter glass transmitting $\lambda >$ 340 nm. Formation of $QuPh^{\bullet}$–NA was confirmed by the change of UV-vis absorption spectra. Next, a deaerated aqueous solution containing Ni-Cu/MOx (0.1 mg) was added to the photoirradiated solution in the dark with stirring. The absorbance change at 420 nm due to $QuPh^{\bullet}$–NA was continuously monitored by UV-vis spectrometer.[29] Evolved H_2 in the headspace of a reaction vial was intermittently quantified by a gas chromatograph.

Acknowledgements

This work was supported by Grants-in-Aid (Nos. 24350069 and 25600025) for Scientific Research from Japan Society for the Promotion of Science (JSPS), an ALCA project from Japan Science and Technology Agency (JST). We sincerely acknowledge the Research Centre for Ultra-Precision Science & Technology, Osaka University for TEM measurements.

Notes and references

[a] *Department of Material and Life Science, Graduate School of Engineering, Osaka University, ALCA and SENTAN, Japan Science and Technology Agency (JST), Suita, Osaka 565-0871, Japan*
E-mail: fukuzumi@chem.eng.osaka-u.ac.jp; yamada@chem.eng.osaka-u.ac.jp

[b] *Department of Applied Chemistry & Bioengineering, Graduate School of Engineering, Osaka City University, 3-3-138 Sugimoto, Sumiyoshi-ku, Osaka, 558-8585, Japan*

[c] *Faculty of Science and Engineering, Meijo University, ALCA and SENTAN, Japan Science and Technology Agency (JST), Nagoya, Aichi 468-0073, Japan*

[d] *Department of Bioinspired Science, Ewha Womans University, Seoul 120-750, Korea*

† Electronic Supplementary Information (ESI) available: DLS measurement (Fig. S1) TEM images (Figs. S2 and 3) See DOI: 10.1039/b000000x/

1 S. Dunn, in *Encyclopedia of Energy*, Elsevier Inc., 2004, vol. 3, pp. 241-252.
2 M. Momirlan and T. N. Veziroglub, *Int. J. Hydrogen Energy*, 2005, **30**, 795-802
3 *The Hydrogen Economy: Opportunities, Costs, Barriers, and R&D Needs*, 2004, U.S. National Research Council and U.S. National Academy of Engineering.
4 G. Laurenczy, *Encyclopedia of Catalysis,* ed. I. T. Horvath, Wiley–Interscience, Hoboken, NJ, 2010.
5 A. K. Hussein, *Renewable Sustainable Energy Rev.*, 2015, **42**, 460-476.
6 J. A. Herron, J. Kim, A. A. Upadhye, G. W. Huber and C. T. Maravelias, *Energy Environ. Sci.*, 2015, **8**, 126-157.
7 J. M. Thomas, *Energy Environ. Sci.*, 2014, **7**, 19-20.
8 S. Berardi, S. Drouet, L. Francas, C. Gimbert-Surinach, M. Guttentag, C. Richmond, T. Stoll and A. Llobet, *Chem. Soc. Rev.*, 2014, **43**, 7501-7519.
9 Z. Han and R. Eisenberg, *Acc. Chem. Res.,* 2014, **47**, 2537–2544.
10 A. J. Cowan and J. R. Durrant, *Chem. Soc. Rev.*, 2013, **42**, 2281-2293.
11 D. G. Nocera, *Acc. Chem. Res*., 2012, **45**, 767–776.
12 M. Wang, L. Chen and L. Sun, *Energy Environ. Sci.*, 2012, **5**, 6763-6778.
13 H. B. Gray, *Nat. Chem*., 2009, **1**, 7–7.
14 V. Artero and M. Fontecave, *Chem. Soc. Rev*., 2013, **42**, 2338–2356.
15 J. J. Concepcion, R. L. House, J. M. Papanikolas and T. J. Meyer, *Proc. Natl. Acad. Sci. U. S. A.,* 2012, **109**, 15560–15564.
16 A. K. Vannucci, L. Alibabaei, M. D. Losego, J. J. Concepcion, F. Kalanyan, G. N. Parsons and T. J. Meyer, *Proc. Natl. Acad. Sci. U. S. A.,* 2013, **110**, 20918–20922.
17 A. J. Cowan and J. R. Durrant, *Chem. Soc. Rev*., 2013, **42**, 2281–2293.
18 S. Fukuzumi, Y. Yamada, T. Suenobu, K. Ohkubo and H. Kotani, *Energy Environ. Sci.*, 2011, **4**, 2754-2766.
19 M. D. Kärkäs, E. V. Johnston, O. Verho and B. Åakermark, *Acc. Chem. Res*., 2014, **47**, 100–111.
20 J. R. McKone, N. S. Lewis and H. B. Gray, *Chem. Mater.,* 2014, **26**, 407–414.
21 H. Ozawa and K. Sakai, *Chem. Commun*., 2011, **47**, 2227–2242.
22 M. Kobayashi, S. Masaoka and K. Sakai, *Angew. Chem., Int. Ed*., 2012, **51**, 7431–7434.
23 N. Wang, M. Wang, L. Chen and L. Sun, *Dalton Trans*., 2013, **42**, 12059–12071.
24 M. Grätzel, *Acc. Chem. Res.,* 1981, **14**, 376–384.
25 Y. Yamada, K. Yano and S. Fukuzumi, *Aust. J. Chem.,* 2012, **65**, 1573–1581.
26 H. Kotani, K. Ohkubo, Y. Takai and S. Fukuzumi, *J. Phys. Chem. B*, 2006, **110**, 24047–24053.
27 H. Kotani, T. Ono, K. Ohkubo and S. Fukuzumi, *Phys. Chem. Chem. Phys*., 2007, **9**, 1487–1492.
28 H. Kotani, R. Hanazaki, K. Ohkubo, Y, Yamada and S. Fukuzumi, *Chem.–Eur. J*., 2011, **17**, 2777–2785.
29 Y. Yamada, T. Miyahigashi, H. Kotani, K. Ohkubo and S. Fukuzumi, *J. Am. Chem. Soc*., 2011, **133**, 16136–16145.
30 Y. Yamada, T. Miyahigashi K. Ohkubo and S. Fukuzumi, *Phys. Chem. Chem. Phys*., 2012, **14**, 10564–10571.
31 Y. Yamada, H. Tadokoro and S. Fukuzumi, *RSC Adv*., 2013, **3**, 25677–25680.
32 Y. Yamada, A. Nomura, H. Tadokoro and S. Fukuzumi, *Catal. Sci. Technol*., 2015, **5**, 428–437.
33 S. Fukuzumi, H. Kotani, K. Ohkubo, S. Ogo, N. V. Tkachenko and H. Lemmetyinen, *J. Am. Chem. Soc.*, 2004, **126**, 1600–1601.
34 H. Kotani, K. Ohkubo, T. and S. Fukuzumi, *Faraday Discuss*., 2012, **155**, 89–102.
35 S. Fukuzumi, K. Ohkubo and T. Suenobu, *Acc. Chem. Res.,* 2014, **47**, 1455–1464.

36 S. Harinipriya and M. V. Sangaranarayanan, *Langmuir*, 2002, **18**, 5572–5578.
37 E. Amouyal and P. Koffi *J. Photochemistry,* 1985, **29**, 227 – 242.
38 P. S. Bassi, Gurudayal, L. H. Wong and J. Barber, *Phys. Chem. Chem. Phys.*, 2014, **16**, 11834–11842.
39 Y. Yamada, S. Shikano and S. Fukuzumi *J. Phys. Chem. C,* 2013, **117**, 13143–13152.
40 Y. Yamada, T, Miyahigashi, H, Kotani, K, Ohkubo and S. Fukuzumi, *Energy Environ. Sci*., 2012, **5**, 6111–6118.
41 Y. Yamada, S. Shikano, T. Akita and S. Fukuzumi, *Catal. Sci. Technol.,* 2015, **5**, 979–988.
42 Y. Zhang, W. Huang, S. E. Habas, J. N. Kuhn, M. E. Grass, Y. Yamada, P. Yang and G. A. Somorjai, *J. Phys. Chem. C,* 2008, **112**, 12092–12095.
43 S. Nishimura, S. Takagaki, S. Maenosono and K. Ebitani, *Langmuir*, 2010, **26**, 478–483.
44 R. W. G. Wyckoff, *Crystal Structures 1*, 1963, 7-83.
45 J. Greeley, T. F. Jaramillo, J. Bonde, I. Chrokendorff, and J. K. Nørskov, *Nat. Mater.*, 2006, **5**, 909–913.
46 H. G. El-Shobaky, *Appl. Catal., A,* 2004, **278**, 1–9.
47 H. G. El-Shobaky, and Y. M. Fahmy, *Appl. Catal., B,* 2006, **63**, 168–177.

Which is the better precursor to be an H_2 evolution catalyst?

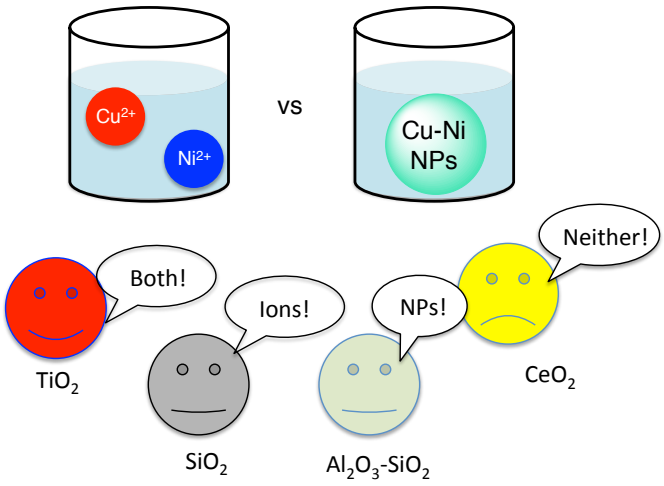

Catalysis of Ni-Cu alloy nanoparticles loaded on various metal oxides for photocatalytic H_2 evolution depends on preparation methods and supports.